JOURNAL OF SPACECRAFT AND ROCKETS
Vol. 35, No. 3, May–June 1998

# Hinge Moment Coefficient Prediction for Nose-Mounted Canard Controls at Supersonic Speeds

Michael G. Landers*
*Dynetics, Inc., Huntsville, Alabama 35806*
and
D. Brian Landrum†
*University of Alabama in Huntsville, Huntsville, Alabama 35899*

**The prediction of nose-mounted canard hinge moments for supersonic rockets poses a unique problem for which the semiempirical methods utilized in rapid aerodynamic prediction codes may not provide sufficient accuracy for preliminary design of the control actuation system. Although providing accurate predictions of canard normal force, such codes generally cannot predict hinge moments effectively due to both their empirical nature and their inability to address the local flowfield conditions on the rocket nose. It is shown that the local flowfield properties must be characterized to accurately determine the longitudinal center of pressure of the canards. A theoretical approach has been developed to predict normal force coefficient, longitudinal center of pressure, and hinge moment coefficient for nose-mounted canards. The method is based on shock-expansion theory and airfoil strip theory and accounts for local flowfield properties, tip pressure losses, and body carryover effects. In contrast to predictions by an industry standard semiempirical code, the new theoretical method consistently estimates canard longitudinal center of pressure with a higher degree of accuracy, resulting in good agreement with experimental hinge moment data for nose-mounted canards at Mach 1.25–2.00.**

## Nomenclature

$A$ = canard aspect ratio
$A_{cs}$ = canard cross-sectional area, in.$^2$
$b$ = canard span (two panels, excluding body), in.
$C_{HM}$ = canard hinge moment coefficient
$C_{hm}$ = airfoil section hinge moment coefficient
$C_N$ = canard normal force coefficient
$C_{N\alpha}$ = slope of canard normal force coefficient vs angle-of-attack curve, 1/deg
$C_n$ = airfoil section normal force coefficient
$C_r$ = canard root chord, in.
$c$ = local airfoil section chord, in.
$d$ = body diameter, in.
$K_{W(B)}$ = wing–body interference factor with angle of attack ($\delta_c$ is 0 deg)
$k_{W(B)}$ = wing–body interference factor with control deflection ($\alpha$ is 0 deg)
$M$ = Mach number
$P$ = static pressure, psi
$P_t$ = total pressure, psi
$q$ = dynamic pressure, psi
$r$ = body radius, in.
$s$ = canard semispan, including body radius, in.
$U$ = uncertainty in experimental result
$X_{CP}$ = canard longitudinal center-of-pressure location measured from leading edge, in.
$X_{HL}$ = canard hingeline location measured from leading edge, in.
$x_{CP}$ = longitudinal center-of-pressure location for airfoil strip measured from leading edge, in.
$x_{HL}$ = hingeline location for airfoil strip measured from leading edge, in.
$y$ = distance along canard semispan, in.
$\alpha$ = angle of attack, deg
$\beta$ = $\sqrt{(M^2 - 1)}$
$\delta_c$, del = canard deflection angle (positive deflection defined by leading edge deflected up), deg
$\gamma$ = canard hingeline skew angle, deg

*Subscripts*

$L$ = local value
$W$ = wing alone
W(B) = wing in presence of body
$\infty$ = freestream reference

Received Aug. 7, 1997; revision received Jan. 7, 1998; accepted for publication Jan. 9, 1998. Copyright © 1998 by the American Institute of Aeronautics and Astronautics, Inc. All rights reserved.

*Aerospace Engineer, Missile Systems. Senior Member AIAA.
†Assistant Professor, Department of Mechanical and Aerospace Engineering, RI E-33. Senior Member AIAA.

## Introduction

INTEGRATION of a low-cost inertial guidance and control package could significantly increase the range and accuracy of existing tube-launched, supersonic free-flight rockets.[1] Such a package utilizing canard controls would provide the advantages of a simple control design with a large control force-to-weight ratio. Most supersonic guided rockets are designed with canard controls located on a cylindrical body section aft of the missile nose. Incorporation of nondeployable, all-movable canards into an existing free-flight rocket would not only require adequate clearance between the canards and the launch tube, i.e., span constrained, but also sufficient packaging volume for the control actuation system (CAS). These requirements may dictate that the canards be positioned along the rocket nose, conformal with the varying radius nose segments. Because the limited packaging volume dictates minimal CAS size, weight, and power, accurate predictions of canard aerodynamics are required. Although several classic textbooks[2–5] and NACA reports[6,7] discuss theoretical approaches for determining the aerodynamic characteristics of control surfaces, they generally do not address nose-mounted canard controls.

Many of the current industry-standard, rapid aerodynamic prediction codes rely on semiempirical methods and empirical databases to predict canard-alone aerodynamics.[8] Slender-body theory[6] is typically utilized to account for canard–body interference, or carryover effects. Experience with codes such as the U.S. Air Force Missile DATCOM 6/93 (Ref. 9) reveals that they do not consistently predict accurate hinge moment coefficients, i.e., within 10%, for nose-mounted canards. Although these codes tend to predict canard normal force to a relatively high degree of accuracy, the longitudinal center of pressure is generally not well predicted. This deficiency is in part due to the semiempirical nature of the codes and

the slender-body theory assumptions. In addition, nose-mounted canards are subject to the local expanding flowfield behind the nose bow shock, which is not accounted for in current prediction techniques.

Noting the deficiencies in the semiempirical prediction codes, Nielsen and Goodwin,[10] Goodwin and Nielsen,[11] and Nielsen[12] developed a method for predicting canard hinge moments. In their approach, semiempirical methods are used to predict canard-alone normal force coefficient and center of pressure for a lifting surface. A theoretical correction for airfoil thickness is then applied to the center of pressure. However, depending on the accuracy of the initial semiempirical estimate of the center-of-pressure location relative to the control hingeline, the thickness correction may, in some cases, actually worsen hinge moment predictions.

The theoretical aspects advanced in the thickness correction of Refs. 10–12 have been expanded to derive a new, nonempirical method to estimate nose-mounted canard aerodynamic characteristics based solely on first principles. This new method, called FINCHM, predicts canard normal force coefficient, longitudinal center of pressure, and hinge moment coefficient. The method is based on shock-expansion and airfoil strip theory, and accounts for local flowfield properties, tip pressure losses, and body carryover effects. Based on comparisons to Missile DATCOM and experimental data, the new method provides more accurate predictions of nose-mounted canard hinge moment coefficients. The technique is robust and could be utilized in the design and development of volume-constrained control actuation systems. A detailed discussion of the FINCHM methodology and capabilities is presented in Ref. 13. This paper summarizes the analyses and highlights key observations from the results.

## Experimental Database

The primary experimental database was obtained in a series of three wind-tunnel tests performed in the early 1970s to investigate the effectiveness of small, nose-mounted canards in providing control for a maneuvering rocket.[14–18] These experimental data have been maintained in the CANARD database,[19] which resides on the U.S. Army Aviation and Missile Command (AMCOM) Aerodynamic Analyzer System.

### Model and Instrumentation

The wind-tunnel model, shown schematically in Fig. 1, consisted of a sting-mounted body of revolution (5-in. diam, 52-in. length) with a pointed 3-caliber tangent ogive nose. The model allowed for a set of four canards to be mounted at three distinct longitudinal positions along the nose (1, 2, and 3) at model stations 6.704, 9.127, and 15.000 in., respectively. As shown in Fig. 2, the canard was defined by a straight-tapered, clipped-delta planform with a modified double-wedge cross section and aspect ratio of 1.154 (canard panel alone).

Individual sets of canards were tested at each position, with the canards mounted flush to the ogive nose. As shown in Figs. 1 and 2, although the planform shape remained constant, the leading and trailing edge sweep angles of the canards (relative to the freestream flow) varied depending on the local body slope at the given mounting position. The balance attachment point for the canards remained perpendicular to the model body centerline at each mounting position. Therefore, canard hinge moments were resolved about the hingeline defined as the centerline of each attachment point. Measured along the root chord, the canard hingeline for each position was located 1.17 in. aft of the canard leading edge.

The model was instrumented with four canard balances to measure aerodynamic forces and moments. The AMCOM-supplied three-component balances measured canard normal force, hinge moment, and root bending moment. Each canard balance was mounted parallel with the model centerline. Remote-controlled electric motors were installed internal to the model to provide independent canard deflections from −5 to 15 deg.

### Facilities and Measurements

The aerodynamic data were obtained from tests in three separate wind-tunnel facilities: the Calspan Transonic Wind Tunnel (Mach

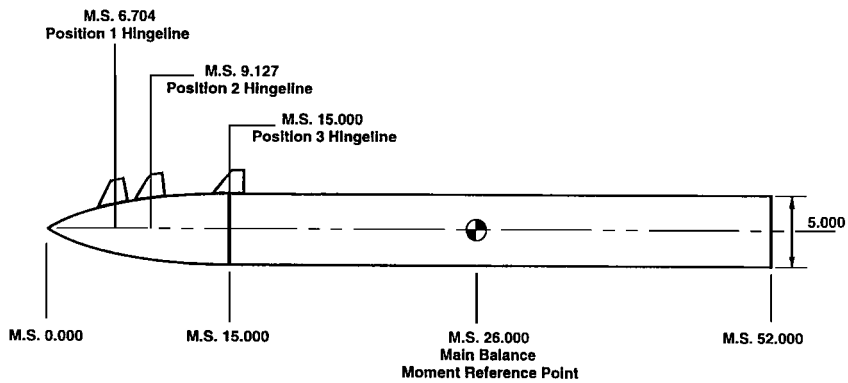


**Fig. 1 Schematic of wind-tunnel test model indicating canard positions.**

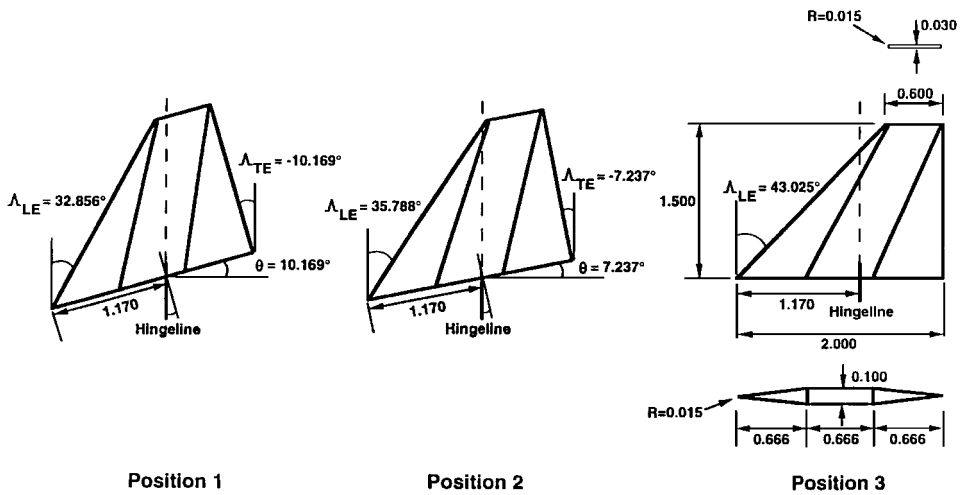


**Fig. 2 Canard geometry and orientation at three positions along the rocket model nose.**

**Table 1 Estimated uncertainties in CANARD experimental data ($\alpha = 10$ deg, $\delta_c = 9$ deg)**

| | | | $U_{Xcp}/C$ root | | |
|---|---|---|---|---|---|
| Mach | $U_{CN}/CN$ | $U_{CHM}$/CHM | Position 1 | Position 2 | Position 3 |
| 1.25 | ±0.0501 | ±0.0501 | ±0.0061 | ±0.0054 | ±0.0052 |
| 1.50 | ±0.0501 | ±0.0501 | ±0.0080 | ±0.0071 | ±0.0053 |
| 2.00 | ±0.0501 | ±0.0501 | ±0.0081 | ±0.0075 | ±0.0054 |

0.6–1.25), the NASA Ames Research Center 6 × 6 ft Supersonic Wind Tunnel (Mach 1.5 and 2.0), and Arnold Engineering Development Center Tunnel A (Mach 1.5–4.5). Data were obtained for both pitch and roll sweeps at angles of attack from −3 to 12 deg with canard deflections from −5 to 15 deg. Aerodynamic coefficients were calculated using the model reference length of 5.00 in., the corresponding reference area of 19.63 in.$^2$, and the tunnel freestream dynamic pressure.

The FINCHM method is currently limited to canards located in the horizontal plane of the rocket. Therefore, a consistent set of pitch-sweep data was obtained from the Calspan and NASA Ames Research Center tests for the canards located in the horizontal plane at three longitudinal positions along the nose. The set consisted of data for canards at Mach 1.25, 1.50, and 2.00; 0–12 deg angle of attack; and 0-, 3-, and 9-deg canard deflection. Both horizontal canards were mutually deflected in the same direction while the vertical canards remained undeflected. Test data were not available to determine canard–canard interference effects.

#### Experimental Uncertainty

With renewed emphasis on assessing data quality and developing standards for wind-tunnel testing, analysis techniques for estimating the uncertainty in experimental measurements have been well documented.[20–24] A rigorous uncertainty analysis[13] was performed for the CANARD experimental data presented in this paper. Estimated uncertainties in model geometric parameters, canard balance force and moment measurements, and tunnel operating conditions were incompletely documented in posttest reports. Therefore, expert sources directly involved with the original tests and familiar with three-component panel balances, similar wind-tunnel models, and the wind-tunnel facilities were consulted to confirm the estimated uncertainties used in the present analysis. Utilizing an error propagation technique based on a Taylor series approach,[21] estimations of the uncertainties in canard normal force coefficient, longitudinal center of pressure, and hinge moment coefficient were determined. Because the uncertainty varies with angle of attack and deflection angle, Table 1 presents maximum uncertainties calculated for the experimental data with balance load conditions at 10-deg angle of attack and 9-deg canard deflection. The resultant uncertainty bands are shown on all subsequent plots of the experimental data.

The wind-tunnel test data are stored in the CANARD database to only four significant digits. For the case of low canard balance loading developed from low tunnel dynamic pressure coupled with a large model reference area, the canard moments become very small and require a minimum of five significant digits. Because of the lack of sufficient significant digits in some of the test cases, the hinge moment data exhibit a stairstep effect with variation in angle of attack. The uncertainties associated with this data-reduction roundoff were not addressed.

## Theoretical Modeling Issues

For canards located on the cylindrical rocket body aft of the nose, it is convenient to assume the flow has expanded back to a nominal freestream value with properties that are uniform along the canard span. In addition, interference between the nose bow shock and the canards is generally not an issue. However, canards mounted on the varying radius nose are inclined to the freestream flow and are subject to the local expanding flowfield behind the bow shock. In extreme cases, the canards may intersect the nose shock wave, which could result in significant gradients in flow properties along the canard span. As described in the following section, the potential for bow-shock/canard interaction was investigated. The local flow conditions were then evaluated including an investigation of the flow regimes that exhibit supersonic leading edges. These analyses helped define modeling issues and limitations that had to be considered in the development of the canard aerodynamic analysis technique.

**Table 2 Local Mach numbers at canard longitudinal positions ($\alpha = 0$ deg)**

| | $M_\infty = 1.25$ | | $M_\infty = 1.50$ | | $M_\infty = 2.00$ | |
|---|---|---|---|---|---|---|
| Position | DATCOM | ZEUS[a] | DATCOM | ZEUS | DATCOM | ZEUS |
| 1 | **1.14**[b] | N/A | 1.38 | 1.36 | 1.82 | 1.80 |
| 2 | **1.22** | N/A | 1.45 | 1.41 | 1.91 | 1.87 |
| 3 | 1.36 | N/A | 1.58 | 1.54 | 2.08 | 2.05 |

[a]Existence of subsonic flow precludes solution.
[b]Boldface indicates subsonic leading-edge condition.

#### Bow-Shock/Canard Interaction

An examination of the experimental data did not reveal a distinct interaction of the nose bow-shock wave with the horizontal canards at angle of attack and canard deflection. To further verify this assumption, the Zonal Euler Solver (ZEUS) code[25,26] was used to characterize the nose shock shape and to compute the local flowfield properties at the three canard positions. Based on pitch-plane symmetry, only half of the axisymmetric ogive/cylinder body was modeled using a single zone defined by a uniform 72 × 36 mesh. The shock-fitting option was used to locate the bow-shock wave in relation to the canards at each of the three mounting locations; at freestream Mach numbers of 1.25, 1.50, 2.00, and 3.00; and at $\alpha = 0$ and 10 deg. The computations for Mach 1.25 failed due to subsonic flow regions in the starting solution. Computed shock shapes revealed no intersection between the bow shock and the canards located at any position along the nose for Mach 1.50 and 2.00.

#### Local Mach Number and Canard Leading-Edge Condition

For canards located in the expanding flow behind the nose bow shock, the local Mach number just ahead of the canards may be significantly different from the freestream Mach number. The body-alone configuration was modeled in both DATCOM and ZEUS at freestream Mach numbers of 1.25, 1.50, and 2.00 and angles of attack 0 and 10 deg. The local surface Mach numbers calculated at each longitudinal canard position and 0-deg angle of attack are shown in Table 2. The differences between DATCOM and ZEUS Mach number estimates are less than 3%. Also, the ZEUS-predicted spanwise Mach number variation along the canard leading edge was less than 5%. With such small variations, the flow along the canard leading edge at each position may be considered uniform and equal to the local surface value. However, due to the significant difference between the local and freestream Mach number for supersonic flow about the ogive nose, it is postulated that the local Mach number relative to the canard must be determined to accurately predict nose-mounted canard aerodynamic characteristics.

A canard supersonic leading-edge condition was determined to exist for local Mach numbers greater than or equal to approximately 1.36. Local Mach numbers less than 1.36 result in a subsonic leading-edge condition and no leading-edge shock wave will be created. Theoretical techniques, such as shock-expansion theory, can only provide aerodynamic predictions for canard configurations characterized by a supersonic leading edge. As noted in Table 2, subsonic leading-edge conditions determined at positions 1 and 2 for a freestream Mach number of 1.25 could not be modeled.

## FINCHM Methodology

Accurate prediction of canard hinge moment is primarily affected by accurate prediction of the canard longitudinal center-of-pressure location relative to the control hingeline. As opposed to semiempirical approaches, a new theoretical hinge moment prediction technique, called FINCHM, was developed based on shock-expansion theory applied to the two-dimensional airfoil section with strip theory applied for the entire canard. This approach offers the capability not only to define exact airfoil sections but also to integrate the section characteristics over the canard planform to provide canard-alone normal force coefficient and center-of-pressure predictions. Such versatility allows for the effects of local Mach number and

airfoil thickness on canard center-of-pressure location to be readily estimated. The canard-alone center of pressure and normal force coefficient are also corrected for canard tip pressure loss and canard–body interference. Such corrections account for three-dimensional effects that are not represented in shock-expansion theory. Last, the relation of the hingeline to the normal force acting at the center of pressure determines the hinge moment for the canard on the rocket nose.

**Generalizations and Limitations**

In the application of FINCHM the following important assumptions are made: 1) supersonic, inviscid, compressible flow; 2) attached shock on canard leading edge, i.e., sharp leading edge; 3) supersonic leading-edge condition; and 4) relatively low angles of attack and canard deflections sufficient for linear aerodynamics ($|\alpha|, |\delta_c| \leq 10$ deg). FINCHM application is also currently restricted to a single canard mounted in the horizontal plane of the rocket nose. It is assumed that the nose shock wave does not intersect the canard and that the canard is located ahead of the influence of body vortices. Canard–canard interference effects are not included.

Based on observations of experimental data trends and ZEUS code predictions, several generalizations and simplifications were incorporated into the theoretical approach. The local flow ahead of a canard is approximately uniform across the semispan and inclined at the same angle as the local body tangent. Thus, the canard inclined on the body at any location along the nose can be modeled as the canard alone having zero trailing-edge sweep with the flow parallel to the canard at zero angle of attack. The actual hingeline is perpendicular to the body centerline. Therefore, as shown in Fig. 2, the hingeline in the canard-alone model is skewed relative to the canard by the local body inclination angle.

**Shock-Expansion and Airfoil Strip Theory**

FINCHM calculations are primarily based on shock-expansion theory.[4,27] The local Mach number $M_L$ of the flow in the nose region aft of the bow shock may be significantly different from the freestream Mach number $M_\infty$ ahead of the bow-shock wave. Therefore, the local flow properties, $M_L$, $P_L$, $P_{tL}$, and $q_L$, are used as freestream conditions in the shock-expansion calculations.

As shown in Fig. 3, the canard planform can be divided into any number of longitudinal two-dimensional airfoil sections or strips, which are composed of a series of $J$ straight line segments ($j = 1, \ldots, J$) on the upper and lower airfoil surface. Each airfoil segment represents a compression or expansion surface for which oblique shock theory and Prandtl–Meyer expansion theory may be applied to characterize the compression/expansion angle, local Mach number, and pressure coefficient. It is assumed that the flow through each region is uniform and independent of the other sections such that no shock reflections/interactions occur. With the pressure distribution determined for each airfoil section, the increments in normal force coefficient and hinge moment coefficient may be calculated.

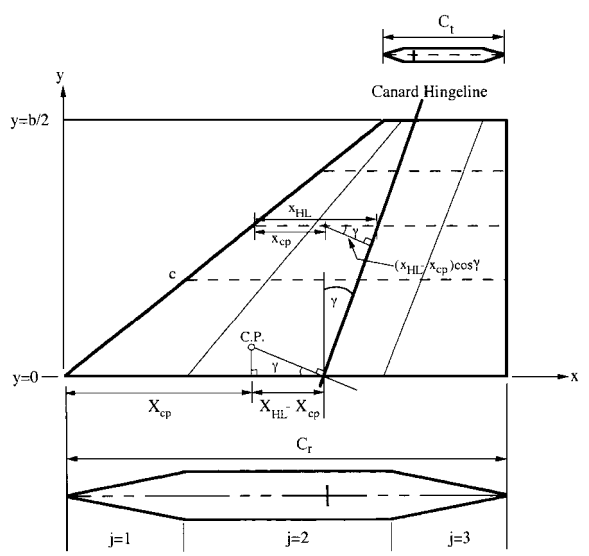


**Fig. 3 Airfoil strip geometry used to determine canard center of pressure and hinge moment.**

The geometric relations used to determine the canard center-of-pressure location and hinge moment are shown in Fig. 3. The locations of the airfoil strip center of pressure and hingeline ($x_{CP}$ and $x_{HL}$) are defined relative to the leading edge of each strip. But the moment arm is perpendicular to the hingeline, not parallel to the strip. Therefore, the moment arm is determined from simple geometric relations with the hingeline skew angle $\gamma$ given by the local surface inclination angle. Because the pressure along the $j$th airfoil segment is considered uniform, the center of pressure is located at the centroid of each airfoil segment. Thus, the moment arm between the hingeline and longitudinal center-of-pressure location for each airfoil strip is obtained from a summation of the segment normal force and hinge moment coefficients by

$$\left[\frac{(x_{HL} - x_{CP})\cos\gamma}{c}\right]_{LE} = \frac{\sum_{j=1}^{J}(C_{hm})_j}{\sum_{j=1}^{J}(C_n)_j} \tag{1}$$

The total canard aerodynamic characteristics are obtained by summation of the aerodynamic characteristics of each airfoil strip. The moment arm for the entire canard in terms of the root chord is calculated by

$$\frac{(X_{HL} - X_{CP})_{LE}}{C_r} = \left(\int_0^{b/2} \frac{c^2}{C_r} C_n \left\{\left[\frac{(x_{HL} - x_{CP})\cos\gamma}{c}\right]_{LE} \mathrm{d}y\right\} \Big/ \int_0^{b/2} (cC_n)\,\mathrm{d}y\right)\cos\gamma \tag{2}$$

The numerator of Eq. (2) is the canard-alone hinge moment coefficient, and the denominator is the normal force coefficient. By specifying the canard hingeline location relative to the leading edge at the root chord, $(X_{HL}/C_r)_{LE}$, the longitudinal center-of-pressure position for the canard alone, $(X_{CP}/C_r)_{LE}$, may also be determined from Eq. (2).

**Canard Tip Effects**

For a canard of finite aspect ratio, a pressure loss occurs in the region of the tip as a result of the pressure differential between the upper and lower surfaces of the canard. In supersonic flow, such pressure losses are limited to the region of influence within the tip Mach cone defined by the local Mach number. For an airfoil section of finite thickness, Bonney[4] has shown that the normal force for the canard of finite aspect ratio may be corrected for tip losses by

$$C_N = (C_N)_{2-D} \times \left(\left(1 - \frac{1}{2\beta A}\right)\left\{1 - 2\left[\frac{0.6M^4 - M^2 + 1}{(M^2 - 1)^{\frac{3}{2}}}\right]\left(\frac{A_{cs}}{c^2}\right)\right\}\right) \tag{3}$$

The correction is applicable for high-aspect-ratio fins and can be applied down to the limiting aspect ratio defined by $1/\beta$.

The decrease in pressure within the tip Mach cone also results in a forward shift in the canard longitudinal center of pressure.[28] For the Mach numbers of interest, the tip Mach cone angles were calculated, the area influenced by each Mach cone was estimated, and the centroid of this area determined. The canard-alone pitching moment about the leading edge was determined from the normal force acting at the center of pressure, neglecting tip effects. Next, the increment in pitching moment due to tip effects was deduced for the normal force increment acting at the area centroid of the Mach cone. The incremental change in pitching moment and normal force resulted in an estimated 2% forward shift in the canard longitudinal center of pressure normalized by the root chord. Therefore, the normalized center of pressure for the canard alone was multiplied by 0.98 to adjust for tip effects. The tip effect corrections applied herein are specific to the configuration of interest and would require recalculation for different canard geometries.

**Corrections for Freestream Mach Number**

For consistent comparison with other aerodynamic code predictions and experimental data, the FINCHM canard aerodynamic characteristics determined for local flow conditions are referenced to the actual freestream flow conditions ahead of the nose bow-shock wave by the equation

$$(C_N)_\infty = (C_N)_L (q_L/q_\infty) \tag{4}$$

**Canard–Body Interference Effects**

The combination of the canard and rocket body results in interference effects that alter the canard-alone aerodynamics. As the body angle of attack increases, the magnitude of the velocity component normal to the body increases. This results in an effective increased angle of attack on the canards known as body carryover interference. Assuming that the interference effects are similar with angle of attack and canard deflection, the normal force coefficient for the canard in the presence of the body may be calculated from the normal force slope by

$$(C_N)_{W(B)} = \left(C_{N_\alpha}\right)_\infty \left(K_{W(B)}\alpha + k_{W(B)}\delta_c\right) \tag{5}$$

The canard–body interference factors with angle of attack, $K_{W(B)}$, and control deflection, $k_{W(B)}$, have been previously estimated using slender-body theory.[6] But this theory is strictly applicable to sharp-nosed, slender bodies with canards mounted on an infinite-length cylindrical section (of uniform diameter) sufficiently aft of the expanding nose section. The theory is also restricted to small angles of attack and canard deflection. The nose-mounted canards are mounted on an expanding section of the nose where the body-radius-to-semispan ratio $(r/s)$ varies along the root chord and the assumption of an infinite cylindrical body is not upheld. Therefore, the validity of slender-body theory estimations of nose-canard interference is suspect.

DATCOM estimates the carryover interference by a modified slender-body theory that includes empirical corrections for angle of attack. The local velocity components in the vicinity of the canard can also be determined from the ZEUS code and used to estimate the carryover interference. The DATCOM predicted values of $K_{W(B)}$ agreed to within 5% of the ZEUS predictions. The values of the body interference factor with canard incidence, $k_{W(B)}$, calculated by slender-body theory were essentially constant and independent of nose position. Based on these comparisons, the DATCOM predicted values for $K_{W(B)}$ and $k_{W(B)}$ were utilized in the FINCHM approach.

Another effect of the body influence on the canard is a shift in the longitudinal center of pressure. Nielsen[2] has concluded that the canard center of pressure in the presence of the body with canard deflection and $\alpha = 0$ deg can be approximated by the canard-alone center of pressure, $(X_{cp}/C_r)_{\delta_c} \approx (X_{cp}/C_r)_W$. However, the shift in canard center of pressure in the presence of the body at angle of attack and $\delta_c = 0$ deg may be obtained from slender-body theory as a function solely of the $r/s$ ratio. Therefore, the canard center of pressure in the presence of the body at angle of attack may be determined by

$$\left(\frac{X_{CP}}{C_r}\right)_\alpha = \left(\frac{X_{CP}}{C_r}\right)_W - \left[\left(\frac{X_{CP}}{C_r}\right)_{W(B)r/s=0} - \left(\frac{X_{CP}}{C_r}\right)_{W(B)r/s}\right] \tag{6}$$

Finally, the hinge moment for the canard in the presence of the body is determined from the normal force coefficient and the longitudinal center of pressure as

$$C_{HM} = \frac{C_r}{d}\left(C_{N_\alpha}\right)\left\{K_{W(B)}\alpha\left[\frac{X_{HL} - (X_{CP})_\alpha}{C_r}\right] + k_{W(B)}\delta_c\left[\frac{X_{HL} - (X_{CP})_{\delta_c}}{C_r}\right]\right\} \tag{7}$$

## Comparison of Experimental Data with FINCHM and DATCOM Predictions

Because of the complexity and repetitiveness of the theoretical methods, FINCHM was coded as a series of Fortran subroutines. For versatility, the subroutines make maximum use of the input variables common to DATCOM. Thus, FINCHM could be easily incorporated into DATCOM to provide an alternate theoretical approach in estimating the aerodynamic characteristics of nose-mounted canards.

The geometric characteristics of the canard were modeled, and the hingeline skew angle at each of the three longitudinal positions along the rocket nose was determined as the local tangent to the nose at the hingeline location. DATCOM estimates of local Mach number at each canard position were input to the FINCHM code along with the corresponding freestream Mach numbers of 1.25, 1.50, and 2.00. As already discussed, DATCOM was also utilized to obtain carryover interference factors. Based on a strip resolution study performed to ascertain prediction convergence, the canard planform was divided into 101 equally spaced airfoil strips. The body–canard configuration geometry was modeled exactly as that of the experimental data with four canards, two horizontal canards mutually deflected in pitch and two vertical canards at zero deflection.

The FINCHM and DATCOM codes were used to predict the normal force coefficient, longitudinal center of pressure, and hinge moment coefficient for the canard configurations shown in Figs. 1 and 2. The resultant predictions are compared with experimental data from the CANARD database in Figs. 4–12. Data are presented for a canard mounted in the horizontal plane for Mach 1.50 at angles of attack from −3 to 12 deg and canard deflections of 0, 3, and 9 deg. Estimated uncertainty bands associated with the experimental data are included in the analysis plots.

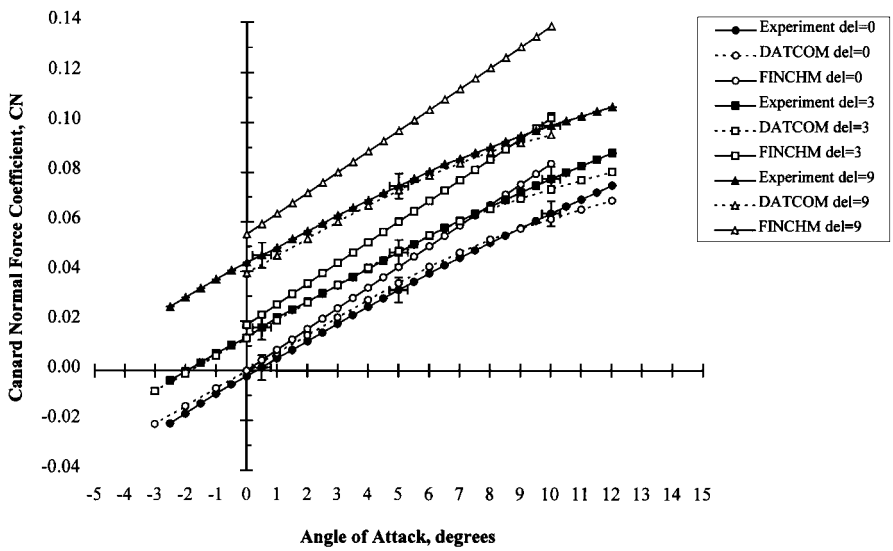


**Fig. 4 Canard normal force coefficient variation with angle of attack: position 1, Mach 1.50.**

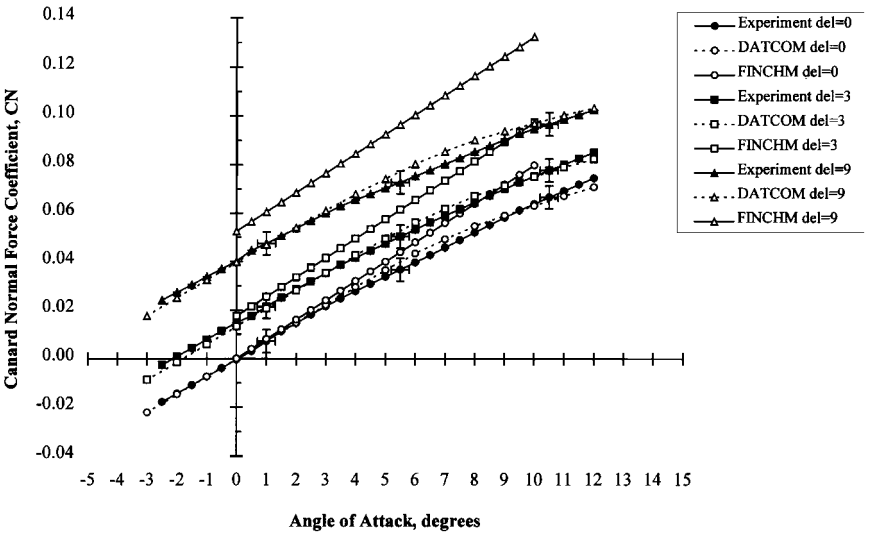


**Fig. 5 Canard normal force coefficient variation with angle of attack: position 2, Mach 1.50.**

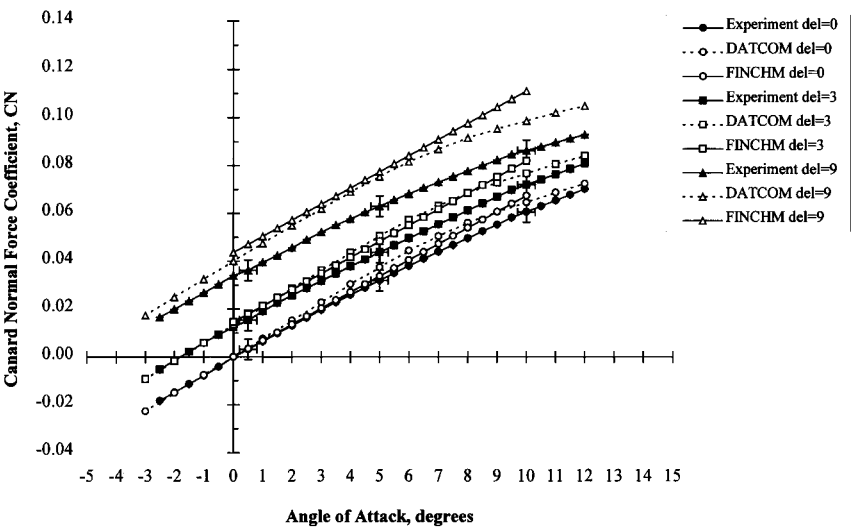


**Fig. 6 Canard normal force coefficient variation with angle of attack: position 3, Mach 1.50.**

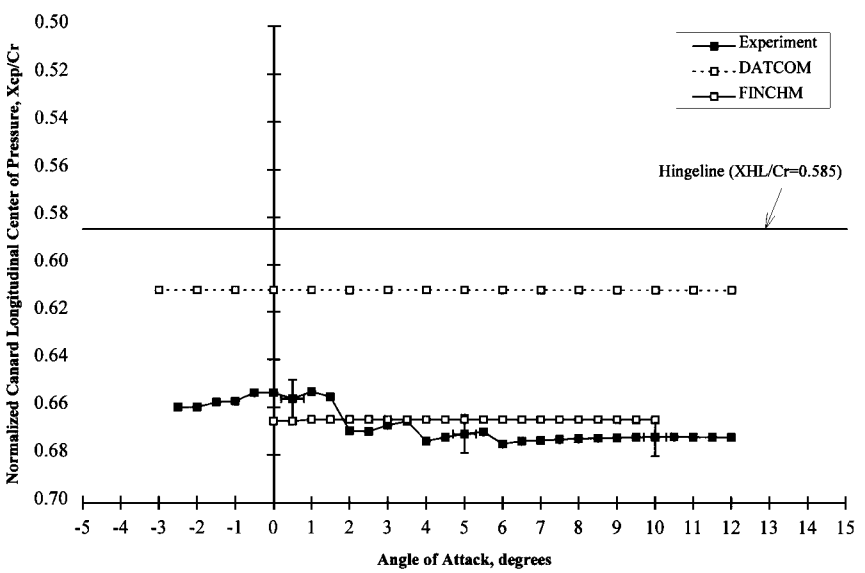


**Fig. 7 Canard center-of-pressure variation with angle of attack: position 1, Mach 1.50.**

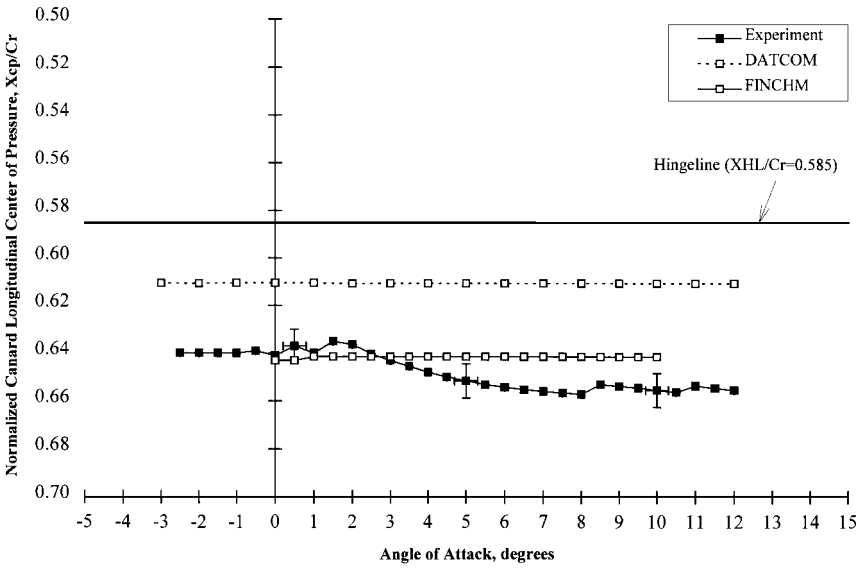


**Fig. 8 Canard center-of-pressure variation with angle of attack: position 2, Mach 1.50.**

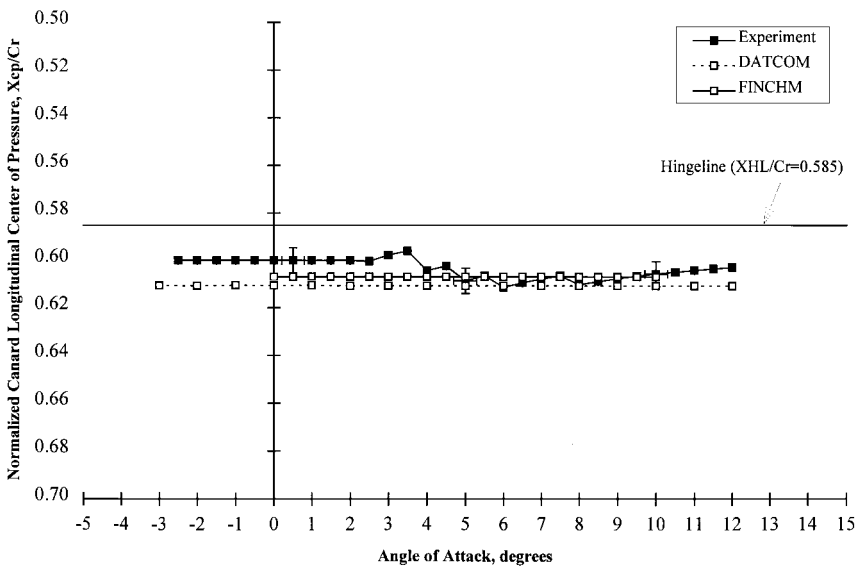


**Fig. 9 Canard center-of-pressure variation with angle of attack: position 3, Mach 1.50.**

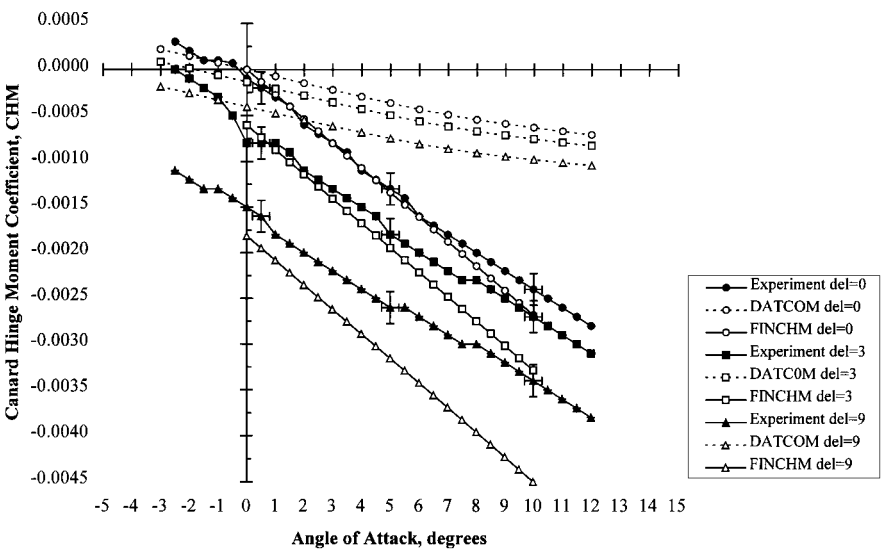


**Fig. 10 Canard hinge moment coefficient variation with angle of attack: position 1, Mach 1.50.**

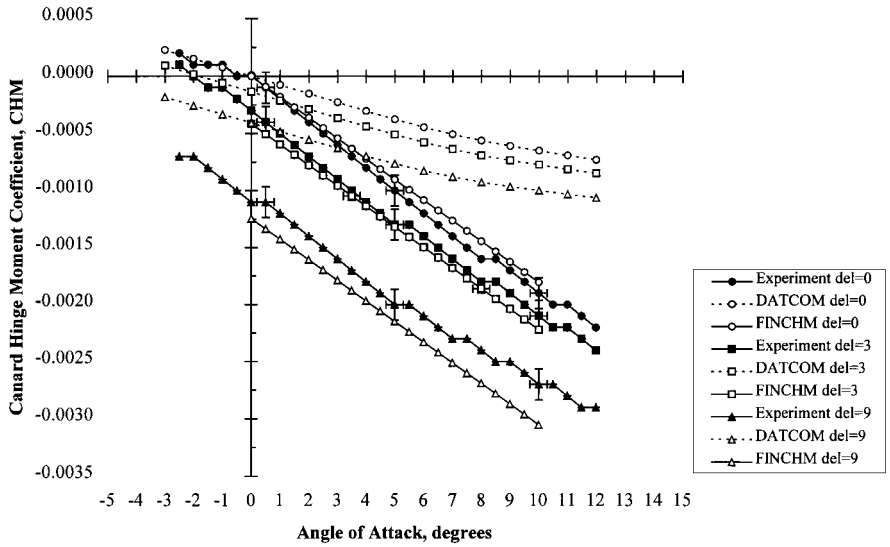


**Fig. 11 Canard hinge moment coefficient variation with angle of attack: position 2, Mach 1.50.**

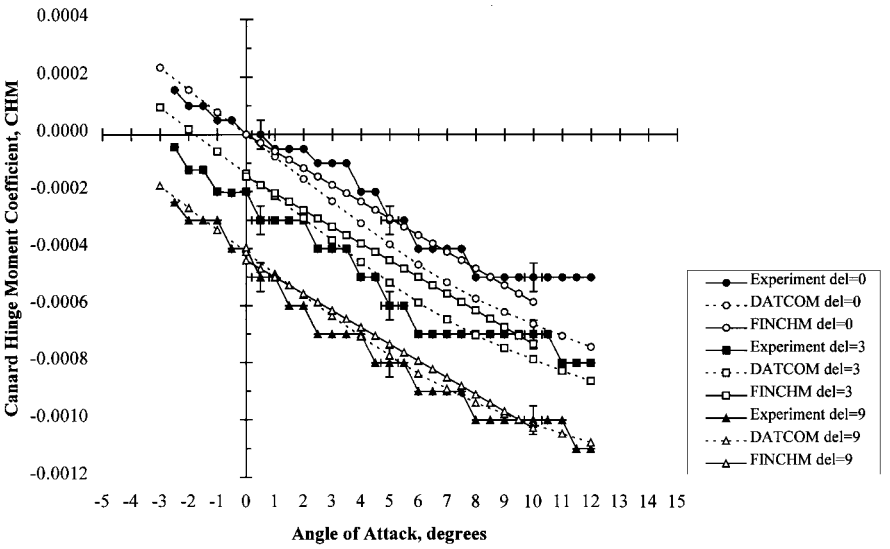


**Fig. 12 Canard hinge moment coefficient variation with angle of attack: position 3, Mach 1.50.**

As shown in Figs. 4–6, the experimental canard normal force coefficient is linear with angle of attack to approximately 10 deg and tends to decrease as the canard moves aft from position 1 to position 3. Canard normal force coefficient also decreases with increasing Mach number at a given canard position. DATCOM predictions of canard normal force coefficient are invariant with canard position because the code does not account for local flow conditions. However, the DATCOM predictions show good agreement with experimental data for all canard deflections and positions except for position 3 and $\delta_c = 9$ deg. FINCHM normal force predictions show fair agreement with data for angles of attack below 5 deg and canard deflections of 0 and 3 deg. As angle of attack and canard deflection is increased, FINCHM overpredicts normal force due to the linear assumptions in the method.

Canard center of pressure was found to be invariant with canard deflection for a given position along the nose. Therefore, comparisons of canard center-of-pressure predictions and data at zero deflection ($\delta_c = 0$ deg) are shown in Figs. 7–9. The experimental canard center of pressure is essentially invariant with angle of attack but noticeably shifts forward from position 1 to position 3. Such shifts in center of pressure may be attributed to variations in canard leading-edge Mach number and sweep angle conditions, which alter the canard pressure distribution at each position along the nose. The FINCHM predictions consistently match experimental data for the three canard positions. The DATCOM predicted center of pressures are invariant with canard position along the nose. DATCOM significantly underpredicts center of pressure at positions 1 and 2 but shows good agreement at canard position 3.

Experimental and predicted canard hinge moment coefficients are compared in Figs. 10–12. Indicative of the canard center-of-pressure location relative to the hingeline, the experimental hinge moment varies significantly with canard position at a constant Mach number. Although FINCHM overpredicts normal force to some degree, its accurate prediction of center of pressure results in generally excellent agreement with the measured hinge moments for all canard positions and deflections. In contrast, DATCOM offers generally accurate predictions of normal force but poor predictions of center of pressure at positions 1 and 2, which results in poor estimations of hinge moment. Only for position 3, where DATCOM center-of-pressure predictions match experimental data, is the predicted hinge moment in good agreement with data. Therefore, the canard hinge moment is shown to be more sensitive to relatively small shifts in longitudinal center-of-pressure location than relatively large changes in canard normal force.

Comparisons were also made between experimental canard aerodynamic data, FINCHM predictions, and DATCOM predictions for position 3 at Mach 1.25 and positions 1–3 at Mach 2.00 (Ref. 13). Similar to the Mach 1.50 results, DATCOM tends to favorably predict normal force, whereas FINCHM provides much better predictions of canard center of pressure and, thus, accurate predictions of hinge moment.

## Conclusions

The accurate determination of canard hinge moment coefficients is necessary for design of future canard-controlled supersonic rockets. But hinge moment is often difficult to ascertain due to the inability to predict the canard longitudinal center-of-pressure location with sufficient accuracy. The aerodynamic characteristics of nose-mounted canards are strongly dependent on local flowfield conditions in the vicinity of the rocket nose shock wave. As opposed to canards mounted on the aft cylindrical section of the body, nose-mounted canards are subject to significant shifts in center of pressure. This behavior may be attributed to variations in canard leading-edge Mach number and sweep angle conditions that alter the canard pressure distribution at each position along the nose. Past investigations have shown that canard hinge moment estimations are more sensitive to relatively small deviations in the center-of-pressure location in relation to the hingeline than relatively large shifts in canard normal force coefficient. It is imperative that canard center of pressure be predicted to the greatest degree of accuracy possible to achieve accurate estimates of canard hinge moment coefficient.

A new, nonempirical method called FINCHM has been developed to predict normal force coefficient, longitudinal center of pressure, and hinge moment coefficient for nose-mounted canards on supersonic rockets. The method, based on fundamental shock-expansion and airfoil strip theory, calculates normal force and center of pressure as functions of the local flowfield properties aft of the nose bow shock. Tip pressure losses and body carryover effects are also taken into account. The new method has been coded in a set of Fortran subroutines that draw on inputs common to the industry-standard Missile DATCOM code.

The FINCHM and semiempirical DATCOM codes were used to predict the normal force coefficients, longitudinal center of pressures, and hinge moment coefficients for several nose-mounted canard configurations at Mach numbers of 1.25, 1.50, and 2.00; angles of attack from −3 to 12 deg; and canard deflections of 0, 3, and 9 deg. The resultant predictions were compared with experimental data from the CANARD database. A detailed assessment of the experimental uncertainty in the data was also performed.

DATCOM produced reasonably accurate predictions of normal force coefficient but generally poor predictions of center of pressure for the nose-mounted canards. The inaccurate prediction of center of pressure resulted in inaccurate hinge moment predictions. The DATCOM values for canard normal force, center of pressure, and hinge moment were also invariant with position on the rocket nose. This behavior is primarily attributed to the fact that DATCOM aerodynamic calculations are based on the freestream rather than local Mach number.

Although the FINCHM method does not predict canard normal force coefficient as accurately as DATCOM, it produces excellent predictions of center of pressure, within 2% of root chord, for all cases investigated. This consistent accuracy in center-of-pressure prediction at each canard position resulted in hinge moment predictions that are in good agreement with experimental data. Such agreement between the FINCHM predictions and experimental data is primarily a result of accounting for the local Mach number and flow properties in the nose region.

Based on the results of this study, it is concluded that the FINCHM method provides improved predictions of nose-mounted canard aerodynamics at supersonic Mach numbers. The method could be easily incorporated into DATCOM to provide more accurate estimation of hinge moment coefficient for canards mounted at various positions along a rocket nose. Although not addressed herein, optimum canard hinge moment coefficient predictions may be obtained by combining DATCOM normal force coefficient predictions with FINCHM center-of-pressure predictions. This approach could be utilized in developing and sizing canard control actuation systems to meet packaging requirements for preliminary design purposes. The method may also be used to provide accurate pretest aerodynamic load estimates for defining future wind-tunnel tests of nose-mounted canard configurations.

## References

[1]Rigby, R. L., "Extended-Range, Guided Rockets Could Counter Long-Range Threats," *ARMY*, Sept. 1996, p. 64.

[2]Nielsen, J. N., *Missile Aerodynamics*, Nielsen Engineering and Research, Inc., Mountain View, CA, 1988, pp. 112–180, 208–250.

[3]Chin, S. S., *Missile Configuration Design*, McGraw–Hill, New York, 1961, pp. 36–47, 162–165.

[4]Bonney, E. A., *Engineering Supersonic Aerodynamics*, McGraw–Hill, New York, 1950, pp. 110–177.

[5]Mendenhall, M. R. (ed.), *Tactical Missile Aerodynamics: Prediction Methodology*, 2nd ed., Vol. 142, Progress in Astronautics and Aeronautics, AIAA, Washington, DC, 1992, pp. 115–169, 379–444.

[6]Pitts, W. C., Nielsen, J. N., and Kaattari, G. E., "Lift and Center of Pressure of Wing–Body–Tail Combinations at Subsonic, Transonic, and Supersonic Speeds," NACA Rept. 1307, 1959.

[7]Goin, K. L., "Equations and Charts for the Rapid Estimation of Hinge Moment and Effectiveness Parameters for Trailing-Edge Controls Having Leading and Trailing Edges Swept Ahead of the Mach Lines," NACA Rept. 1041, 1951.

[8]"Aerodynamic Analysis for Missiles—Evaluation of Aerodynamic Prediction Methods," U.S. Air Force Wright Lab., AFWAL-TR-82-3038, Wright–Patterson AFB, OH, June 1982.

[9]Burns, K. A., Deters, K. J., Stoy, S. L., Vukelich, S. R., and Blake, W. B., "Missile DATCOM User's Manual—Revision 6/93," U.S. Air Force Wright Lab., WL-TR-93-3043, Wright–Patterson AFB, OH, June 1993.

[10]Nielsen, J. N., and Goodwin, F. K., "Preliminary Method for Estimating Hinge Moments of All-Movable Controls," Nielsen Engineering and Research, Inc., NEAR TR 268, Mountain View, CA, March 1982.

[11]Goodwin, F. K., and Nielsen, J. N., "Determination of Optimum Fin Planform and Airfoil Section for Minimizing Fin Hinge Moment," Nielsen Engineering and Research, Inc., NEAR TR 286, Mountain View, CA, Feb. 1983.

[12]Nielsen, J. N., "Aerodynamic Characteristics of Missile Controls," *AGARD Special Course on Aerodynamic Characteristics of Controls*, AGARD Rept. 711, March 1983, pp. 10.1–10.53.

[13]Landers, M. G., "Prediction of Hinge Moment Coefficients for Nose-Mounted Canard Controls at Supersonic Speeds," U.S. Army Aviation and Missile Command, TR CR-RD-SS-97-49, Redstone Arsenal, AL, Aug. 1997.

[14]Burt, J. R., Jr., "An Experimental Investigation of the Aerodynamic Characteristics of Several Nose-Mounted Canard Configurations at Transonic Mach Numbers," U.S. Army Missile Command, TR RD-75-2, Redstone Arsenal, AL, Aug. 1974.

[15]Burt, J. R., Jr., "An Experimental Investigation of the Aerodynamic Characteristics of Several Nose-Mounted Canard Configurations at Supersonic Mach Numbers," U.S. Army Missile Command, TR RD-75-17, Redstone Arsenal, AL, Jan. 1975.

[16]Hemsch, M. J., and Nielsen, J. N., "Test Report for Canard Missile Tests in Ames 6- by 6-Foot Supersonic Wind Tunnel," Nielsen Engineering and Research, Inc., NEAR TR 72, Mountain View, CA, Aug. 1974.

[17]Burt, J. R., Jr., "An Experimental Investigation of the Aerodynamic Characteristics of Nose-Mounted Canard Configurations at Supersonic Mach Numbers (1.5 Through 4.5)," U.S. Army Missile Command, TR RD-77-5, Redstone Arsenal, AL, Oct. 1976.

[18]Burt, J. R., Jr., "Pre-Test Information for a Supersonic Investigation of a Model with Nose Mounted Canard Wings (AEDC)," U.S. Army Missile Command, Internal TN RD-76-1, Redstone Arsenal, AL, Sept. 1975.

[19]Chafin, J. M., "User's Guide for Canard Control (*CANARD*) Aerodynamic Database," New Technology, Inc., Interim TR 1014, Huntsville, AL, June 1979.

[20]Coleman, H., and Stern, F., "Uncertainties and CFD Code Validation," *Journal of Fluids Engineering*, Vol. 119, Dec. 1997, pp. 795–803.

[21]Coleman, H. W., and Steele, W. G., Jr., *Experimentation and Uncertainty Analysis for Engineers*, Wiley, New York, 1989, pp. 40–58.

[22]Fluid Dynamics Panel Working Group 15, "Quality Assessment for Wind Tunnel Testing," AR-304, AGARD, July 1994.

[23]Clark, E. L., "Error Propagation Equations for Estimating the Uncertainty in High-Speed Wind Tunnel Test Results," AIAA Paper 94-2588, June 1994.

[24]Cahill, D. M., "Experiences with Uncertainty Analysis Application in Wind Tunnel Testing," AIAA Paper 94-2586, June 1994.

[25]Wardlaw, A. B., Jr., and Davis, S. F., "A Second Order Godunov Method for Supersonic Tactical Missiles," U.S. Naval Surface Warfare Center, NSWC TR 86-506, Dahlgren, VA, Dec. 1986.

[26]Wardlaw, A. B., Jr., and Priolo, F. J., "Applying the ZEUS Code," U.S. Naval Surface Warfare Center, NSWC TR 86-508, Dahlgren, VA, Dec. 1986.

[27]Ames Research Staff, "Equations, Tables and Charts for Compressible Flow," NACA Rept. 1135, 1953.

[28]Hoak, D. E., and Finck, R. D., "USAF Stability and Control DATCOM," Vol. 2, Sec. 4, U.S. Air Force Wright Lab., Wright–Patterson AFB, OH, April 1978, pp. 4.1.4.3–17.

J. R. Maus
*Associate Editor*